THE JOURNAL OF CELL BIOLOGY

# IFT20 modulates ciliary PDGFRα signaling by regulating the stability of Cbl E3 ubiquitin ligases

Fabian Marc Schmid,[1]* Kenneth Bødtker Schou,[1]* Martin Juel Vilhelm,[1] Maria Schrøder Holm,[1] Loretta Breslin,[1,3] Pietro Farinelli,[1] Lars Allan Larsen,[2] Jens Skorstengaard Andersen,[3] Lotte Bang Pedersen,[1] and Søren Tvorup Christensen[1]

[1]Department of Biology, Section of Cell Biology and Physiology and [2]Wilhelm Johannsen Centre for Functional Genome Research, Department of Cellular and Molecular Medicine, University of Copenhagen, Copenhagen, Denmark
[3]Department of Biochemistry and Molecular Biology, University of Southern Denmark, Odense, Denmark

Primary cilia have pivotal roles as organizers of many different signaling pathways, including platelet-derived growth factor receptor α (PDGFRα) signaling, which, when aberrantly regulated, is associated with developmental disorders, tumorigenesis, and cancer. PDGFRα is up-regulated during ciliogenesis, and ciliary localization of the receptor is required for its appropriate ligand-mediated activation by PDGF-AA. However, the mechanisms regulating sorting of PDGFRα and feedback inhibition of PDGFRα signaling at the cilium are unknown. Here, we provide evidence that intraflagellar transport protein 20 (IFT20) interacts with E3 ubiquitin ligases c-Cbl and Cbl-b and is required for Cbl-mediated ubiquitination and internalization of PDGFRα for feedback inhibition of receptor signaling. In wild-type cells treated with PDGF-AA, c-Cbl becomes enriched in the cilium, and the receptor is subsequently ubiquitinated and internalized. In contrast, in IFT20-depleted cells, PDGFRα localizes aberrantly to the plasma membrane and is overactivated after ligand stimulation because of destabilization and degradation of c-Cbl and Cbl-b.

## Introduction

Platelet-derived growth factor receptor α (PDGFRα) is a receptor tyrosine kinase that controls a series of cellular processes, including proliferation, survival, migration, and differentiation, in turn affecting development and tissue homeostasis of several organs. Consequently, aberrant PDGFRα signaling contributes to the pathophysiology of various diseases and developmental disorders, such as fibrotic diseases, tumorigenesis, and cancer (Olson and Soriano, 2009; Demoulin and Montano-Almendras, 2012; Heldin and Lennartsson, 2013; Demoulin and Essaghir, 2014; Velghe et al., 2014; Farahani and Xaymardan, 2015).

PDGFRα localizes to, and is activated at, the primary cilium in a variety of cell types (Christensen et al., 2017). In fibroblasts, ciliary PDGFRα signaling involves the activation of AKT and ERK1/2 at the ciliary base to control directional cell migration (Schneider et al., 2005, 2009, 2010; Clement et al., 2013). PDGFRα is up-regulated during concomitant growth arrest and formation of the primary cilium, and up-regulation and activation of the receptor by PDGF-AA are blocked in cycling cells and in growth-arrested mouse embryonic fibroblasts lacking intraflagellar transport (IFT) proteins IFT88 (Schneider et al., 2005) or IFT172 (Umberger and Caspary, 2015), which are part of the IFT-B subcomplex required for ciliogenesis (Taschner et al., 2016). These findings indicate that the basal pool of PDGFRα in cycling cells is not accessible at the plasma membrane for ligand-mediated receptor activation but needs to be localized to the cilium for normal signal transduction. However, the mechanisms by which PDGFRα localizes to the primary cilium and how the level of PDGFRα signaling at the cilium is properly balanced by feedback inhibition after ligand-induced activation of the receptor are unknown.

To study the mechanisms that regulate sorting and feedback inhibition of ciliary PDGFRα signaling, we investigated the role of IFT20, which is part of the ciliary IFT-B subcomplex (Cole et al., 1998; Taschner et al., 2016). In addition, IFT20 localizes to the Golgi compartment to promote vesicular transport of selected transmembrane proteins, including polycystin-2 and opsin, to the primary cilium (Follit et al., 2006, 2008; Keady et al., 2011). IFT20 has also been assigned extraciliary functions, such as organization of the polarized trafficking of T cell receptors (TCRs) to the immune synapse (Finetti et al., 2009, 2014; Vivar et al., 2016) and trafficking procollagen from the endoplasmic reticulum to the Golgi in osteoblasts (Noda et al., 2016). To study the function of IFT20 in regulating PDGFRα signaling, we generated an NIH3T3-based cell line that allows conditional silencing of IFT20 by doxycycline (Dox)-inducible expression of a shRNA targeting mouse IFT20 (NIH3T3$^{shIFT20}$). Using this approach, in which the expression of IFT20 can be down-regulated in a controlled manner, we identified IFT20

*F.M. Schmid and K.B. Schou contributed equally to this paper.

Correspondence to Søren Tvorup Christensen: stchristensen@bio.ku.dk



The Rockefeller University Press
J. Cell Biol. Vol. 217 No. 1 151–161
https://doi.org/10.1083/jcb.201611050

as a novel regulator of ciliary signaling, which interacts with E3 ubiquitin ligases c-Cbl and Cbl-b that mediate ubiquitination and internalization of PDGFRα for feedback inhibition of receptor signaling. IFT20 exerts its effect through the stabilization of the Cbl proteins, which, in the absence of IFT20, undergo autoubiquitination and proteasomal degradation, leading to aberrant PDGFRα signaling.

## Results and discussion

### Conditional silencing of IFT20 leads to defects in feedback inhibition of PDGFRα signaling

To investigate the role of IFT20 in regulating PDGFRα signaling, we first depleted IFT20 by Dox treatment of NIH3T3$^{sh\textit{IFT20}}$ cells (Fig. 1 a), which led to undetectable levels of IFT20 protein after 3 d of treatment, as assessed by Western blot (WB; Fig. 1 b) and immunofluorescence microscopy (IFM) analyses (Fig. 1, c and d). Dox-mediated IFT20 knockdown significantly decreased the frequency of ciliated cells (Fig. 1, e and f), as expected (Follit et al., 2006, 2008; Keady et al., 2011), whereas untreated NIH3T3$^{sh\textit{IFT20}}$ cells displayed normal ciliation frequencies (~60%; Fig. 1 f; Schneider et al., 2005) and showed WT localization of IFT20 at the cilium and at the Golgi complex (Fig. 1, c–e). The Golgi complex was not grossly disturbed in NIH3T3$^{sh\textit{IFT20}}$ cells treated with Dox, as revealed by staining for giantin (Fig. 1 d). To monitor how IFT20 affects the strength and kinetics in feedback inhibition of PDGFRα signaling, we next subjected growth-arrested NIH3T3$^{sh\textit{IFT20}}$ cells to PDGF-AA stimulation for an expanded interval (0–240 min). Interestingly, IFT20-depleted cells displayed a dramatically amplified and prolonged phosphorylation of PDGFRα, AKT, and ERK1/2 as compared with control cells (Fig. 1, g and h), suggesting that feedback inhibition of PDGFRα signaling is impaired in those cells. Importantly, Dox treatment itself did not elicit changes in PDGFRα signaling in WT NIH3T3 cells (Fig. S1, a and b), and we furthermore found that stable expression of a GFP-tagged IFT20 allele, resistant to the IFT20 shRNA (NIH3T3$^{sh\textit{IFT20}\text{-Res}}$; Fig. 1, i and j), rescued the ciliogenesis (Fig. 1 j) and PDGFRα signaling defects in Dox-treated NIH3T3$^{sh\textit{IFT20}}$ cells (Fig. 1, k and l), substantiating the conjecture that IFT20 is required for proper feedback inhibition of signaling. Our results also showed that up-regulation of PDGFRα expression during growth arrest (Schneider et al., 2005) is not affected by IFT20 depletion (Fig. S1 c). This is in sharp contrast to the reduced PDGFRα levels observed in cells lacking IFT88 (Fig. S1 d; Schneider et al., 2005). Thus, IFT20 is essential for proper feedback inhibition of PDGFRα signaling but is not essential for up-regulation and activation of the receptor during growth arrest.

### IFT20 is required for ubiquitination and internalization of PDGFRα

We noticed that overactivation of PDGFRα signaling in Dox-treated NIH3T3$^{sh\textit{IFT20}}$ cells was associated with a prominent reduction in posttranslational modification (PTM) of PDGFRα, as indicated by a major reduction in a high–molecular-weight smear appearing after 10, 30, and 90 min of PDGF-AA stimulation (Fig. 1 g). Because PTM, in response to ligand stimulation, is a distinctive sign of RTK ubiquitination, which leads to internalization and down-regulation of signaling (Coats et al., 1994; Mori et al., 1995), we next monitored the covalent attachment of endogenous or Myc-tagged ubiquitin to PDGFRα by immunoprecipitation (IP) in NIH3T3$^{sh\textit{IFT20}}$ cells stimulated with PDGF-AA for 10 min in the absence or presence of Dox. The results revealed a prominent reduction in receptor polyubiquitination in IFT20-depleted cells (Fig. 2 a), demonstrating that IFT20 is required for proper receptor ubiquitination. In support of that conclusion, restoration of normal PDGFRα signaling in Dox-treated NIH3T3$^{sh\textit{IFT20}\text{-Res}}$ cells was similarly associated with restoration of PTM in PDGFRα (Fig. 1 k), and the activated receptor in Dox-treated, WT NIH3T3 cells displayed neither reduced PTM (Fig. S1 a) nor reduced ubiquitination (Fig. S2 a).

To further examine whether reduced ubiquitination of PDGFRα in IFT20-depleted cells is accompanied by reduced internalization of the receptor, PDGFRα was biotin-labeled using membrane-impermeable EZ-Link Sulfo-NHS-SS-Biotin reagent before or after addition of PDGF-AA. Biotin-labeled proteins were enriched by pull-down with streptavidin beads, followed by WB analysis with an antibody against PDGFRα. In the absence of the ligand, the level of biotinylated receptor at the cell surface and in internalized vesicles was similar in NIH3T3$^{sh\textit{IFT20}}$ cells with or without Dox treatment. Upon addition of PDGF-AA, removal and internalization of PDGFRα from the cell surface was significantly delayed in cells lacking IFT20 (Fig. 2, b and c). Together, these findings indicate that IFT20 is important for ubiquitination and internalization of PDGFRα for proper feedback inhibition of PDGFRα signaling.

### Silencing of IFT20 promotes autoubiquitination and proteasomal degradation of Cbl proteins

Overactivation of PDGFRα and markedly reduced PDGFRα polyubiquitination and internalization upon ligand stimulation in IFT20-deficient cells point to a crucial function of IFT20 in establishing a competent E3-ubiquitin ligase-dependent, negative feedback mechanism in PDGFRα signaling. Because PDGF receptors are bona fide substrates of two proximal RING finger E3-ubiquitin ligase paralogs, designated as c-Cbl and Cbl-b (Bonita et al., 1997; Miyake et al., 1998; Mohapatra et al., 2013), we asked whether the activity or expression of these Cbl proteins was affected in IFT20-depleted cells. First, we found that Cbl-b protein levels are up-regulated upon serum starvation–induced ciliogenesis in NIH3T3 and retinal pigmented epithelial (RPE) 1 cells, whereas the level of c-Cbl was unaffected by serum depletion (Fig. 3 a), suggesting that Cbl-b may carry out specific functions associated with growth arrest or ciliary signaling events or both. Time-course experiments in NIH3T3$^{sh\textit{IFT20}}$ cells revealed that c-Cbl and Cbl-b levels declined concomitant with the reduction in IFT20 levels. The levels of c-Cbl and Cbl-b were significantly reduced after 2 d of Dox treatment and were barely detectable after 6 d (Fig. 3 b). Likewise, reduced levels of c-Cbl were also detected in human embryonic kidney (HEK) 239T cells transfected with shRNA against IFT20 (Fig. S2 b). In contrast, protein levels of those ubiquitin ligases were largely unaffected in WT NIH3T3 cells subjected to siRNA-mediated depletion of IFT88 (Fig. S2 c) as well as in knockout mouse embryonic fibroblasts lacking IFT172 or the kinesin II motor subunit Kif3a (Fig. S2 d), both required for formation of primary cilia (Taschner and Lorentzen, 2016). Therefore, the effect of IFT20 depletion on Cbl protein stability seems not to be solely a consequence of ciliary loss. Further, the reduction in c-Cbl and Cbl-b levels in

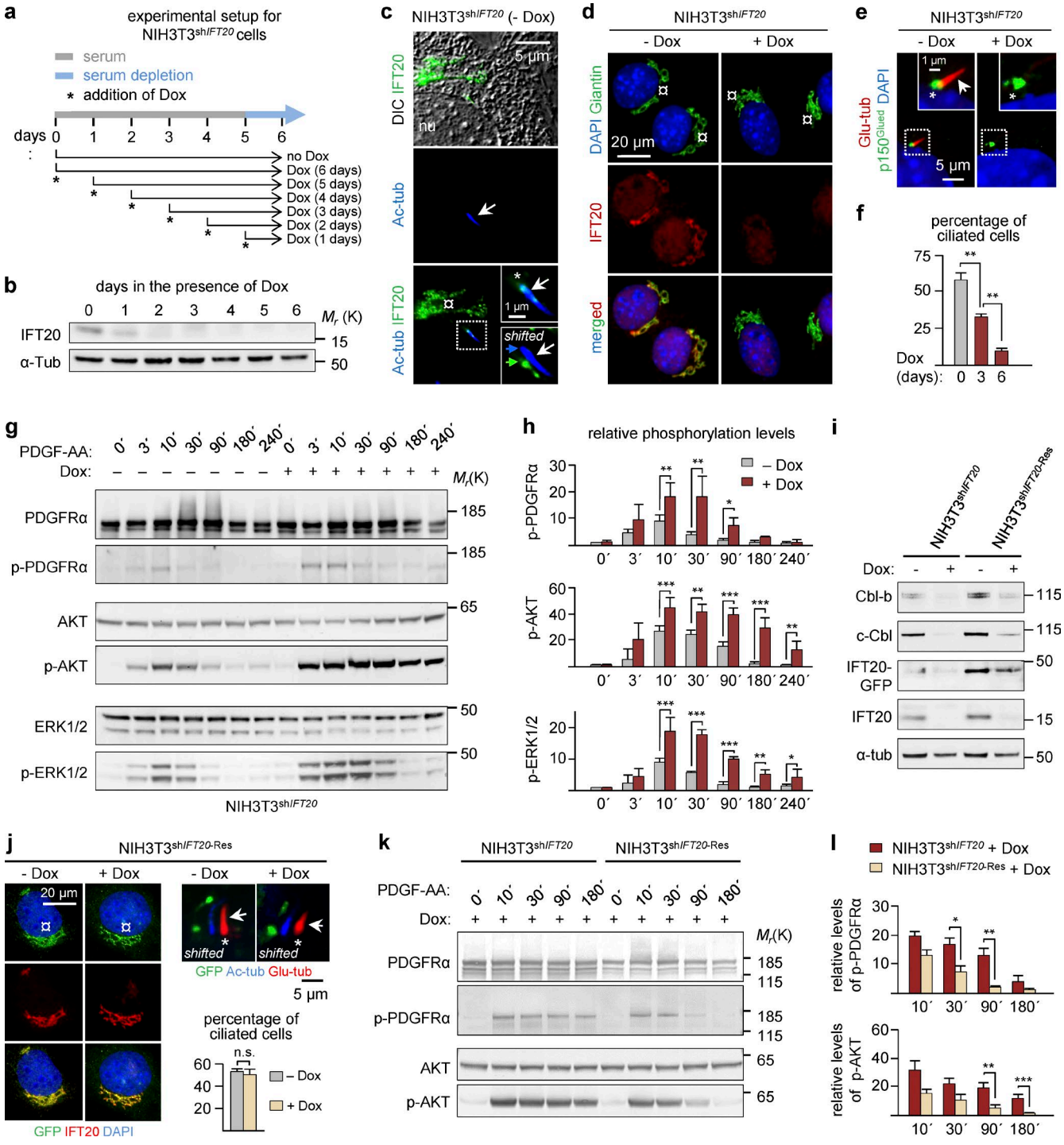


Figure 1. **Conditional gene silencing of IFT20 is associated with defects in termination of PDGFRα signaling. (a)** Experimental setup to verify IFT20 silencing efficiency in NIH3T3$^{shIFT20}$ cells upon treatment with Dox for given times. All cells were grown for 6 d. Asterisks indicate day of Dox addition. **(b)** WB analysis showing IFT20 expression in NIH3T3$^{shIFT20}$ cells during 0–6 d of Dox treatment using the experimental setup outlined in panel a. **(c–e)** IFM images of growth-arrested NIH3T3$^{shIFT20}$ cells treated without (– Dox) or with Dox (+ Dox) for 6 d, showing cellular localization of IFT20. Primary cilia (arrows) were labeled with anti–acetylated α-tubulin (Ac-tub) or anti-detyrosinated α-tubulin (Glu-tub), and the ciliary base/centrosome was labeled with anti–p150$^{glued}$ (asterisks). Nuclei (nu) were visualized with DIC microscopy or DAPI staining. Anti–Giantin was used to label the Golgi complex (dashed line). **(f)** Percentage of ciliated NIH3T3$^{shIFT20}$ cells after Dox treatment, as indicated. Error bars represent means ± SEM ($n$ = 3). **(g)** WB analysis of phosphorylation of PDGFRα (p-PDGFRα), AKT (p-AKT), and ERK1/2 (p-ERK1/2) upon stimulation with PDGF-AA for indicated times in growth-arrested NIH3T3$^{shIFT20}$ cells treated with or without Dox treatment for 6 d. **(h)** Quantification of protein phosphorylations shown in panel g. Error bars represent means ± SEM ($n$ = 3). **(i)** WB analysis of c-Cbl and Cbl-b levels in growth-arrested NIH3T3$^{shIFT20}$ cells as well as in cells stably expressing siRNA-resistant, GFP-tagged IFT20 (NIH3T3$^{shIFT20\text{-}Res}$) after Dox treatment for 6 d. **(j)** IFM analysis of NIH3T3$^{shIFT20\text{-}Res}$ cells with or without Dox treatment for 6 d. Cells were stained with antibodies against GFP and IFT20, and cell nuclei were visualized with DAPI staining. Primary cilia (arrows) were labeled with anti–Glu-Tub and anti–Ac-tub and are shown as shifted overlays. Quantification of ciliated NIH3T3$^{shIFT20\text{-}Res}$ cells; error bars represent means ± SEM ($n$ = 3). **(k)** WB analysis of phosphorylation of PDGFRα (p-PDGFRα) and AKT (p-AKT) upon stimulation with 50 ng/ml PDGF-AA for indicated times in growth-arrested NIH3T3$^{shIFT20}$ versus NIH3T3$^{shIFT20\text{-}Res}$ cells, both treated with Dox for 6 d. **(l)** Quantification of protein phosphorylations shown in panel k. Error bars represent means ± SEM ($n$ = 3).

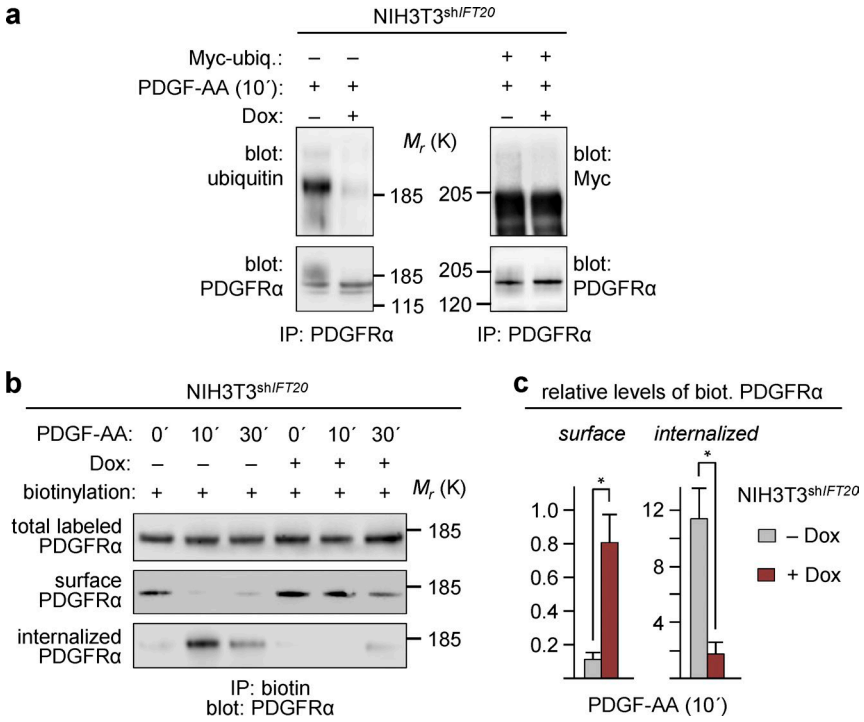


Figure 2. **Conditional gene silencing of IFT20 inhibits ubiquitination and internalization of PDGFRα.** **(a)** PDGFRα ubiquitination upon stimulation with PDGF-AA for 10 min in growth-arrested NIH3T3$^{shIFT20}$ cells cultured with or without Dox for 6 d before ligand addition. IP with anti–PDGFRα was performed on lysates of cells not transfected (left) or transfected with a construct expressing Myc-tagged ubiquitin (right), and IPs were analyzed by WB using antibodies against mono- and polyubiquitin or Myc, respectively. The experiments were repeated three times, and results from one representative experiment are shown. **(b)** WB analysis of surface-biotinylated PDGFRα upon stimulation with PDGF-AA for indicated times in growth-arrested NIH3T3$^{shIFT20}$ cells treated with or without Dox for 6 d. Cell surface proteins were labeled with biotin before (internalized) or after (surface) stimulation with PDGF-AA, followed by IP with streptavidin beads. To detect internalized PDGFRα specifically, extracellular biotin was removed after stimulation with an alkaline glutathione solution. **(c)** Quantification of protein-band intensity for experiment shown in panel b. Error bars represent means ± SEM ($n$ = 3).

Dox-treated NIH3T3$^{shIFT20}$ cells was a specific consequence of the IFT20 depletion because Cbl protein levels could be significantly restored in Dox-treated NIH3T3$^{shIFT20\text{-Res}}$ cells (Fig. 1 i), and no decrease in their levels could be observed in Dox-treated WT NIH3T3 cells (Fig. S2 e). Moreover, NIH3T3$^{shIFT20}$ cells that had been serum starved before IFT20 depletion showed a similar reduction in c-Cbl levels after 6 d of Dox treatment (Fig. S2, f and g), indicating that the observed decline in c-Cbl protein levels was not secondary to cell cycle defects. In addition, knockdown of c-Cbl by siRNA in WT NIH3T3 and RPE-1 cells reduced IFT20 protein levels (Fig. 3 c), without decreasing the level of *Ift20* mRNA (Fig. S2 h), supporting the conclusion of a functional and biochemical interdependence between IFT20 and c-Cbl on the protein level.

Assessment of mRNA levels by quantitative, real-time PCR revealed no significant difference between *c-Cbl* and *Cbl-b* mRNA levels from untreated versus Dox-treated (for 6 d) NIH3T3$^{shIFT20}$ cells (Fig. 3 d), highlighting that reduced amounts of Cbl proteins in IFT20-depleted cells manifest at a posttranscriptional level. Because c-Cbl can modulate its own turnover by a negative feedback mechanism that involves autoubiquitination (Ryan et al., 2006), we studied whether cellular loss of IFT20 triggers autoubiquitination and proteasomal degradation of c-Cbl. Blocking proteasomal degradation by the addition of MG-132 substantially restored the amount of c-Cbl in Dox-treated NIH3T3$^{shIFT20}$ cells, whereas lysosomal inhibition by $NH_4Cl$ showed no obvious effect (Fig. 3 e). Supportively, IFT20 depletion caused excessive c-Cbl polyubiquitination, evident by the increase in low-mobility ubiquitin species in c-Cbl immunoprecipitates, which was paralleled by a concomitant reduction in c-Cbl protein (Fig. 3 f). To investigate whether c-Cbl degradation was a result of autoubiquitination, we generated two NIH3T3$^{shIFT20}$ cell lines that stably expressed human FLAG–tagged WT c-Cbl (NIH3T3$^{shIFT20,\text{FLAG–c-Cbl-WT}}$) or RING-finger mutant c-Cbl (NIH3T3$^{shIFT20,\text{FLAG–c-Cbl,*RING}}$). When IFT20 was depleted, FLAG-tagged, WT c-Cbl was depleted to an extent similar to the corresponding, endogenous c-Cbl protein, whereas the stability of RING-mutated c-Cbl remained unaffected (Fig. 3 g), demonstrating that the process leading to c-Cbl degradation requires its innate enzyme activity. Further, because the ability of Cbl proteins to form dimers is crucial to establish a negative-feedback response to activated PDGFRα signaling (Kozlov et al., 2007; Peschard et al., 2007), we evaluated whether c-Cbl could dimerize in the absence of IFT20. Therefore, we transiently expressed GFP-tagged RING-mutant c-Cbl (GFP-c-Cbl$^{*RING}$) in NIH3T3$^{shIFT20,\text{FLAG–c-Cbl*RING}}$ cells and monitored the amount of GFP-tagged c-Cbl$^{*RING}$ in FLAG immunoprecipitates under untreated and Dox-treated conditions. Thereby, a change in the amount of GFP-tagged c-Cbl$^{*RING}$ could be assessed, independent of autoubiquitination and degradation of the protein. We found that c-Cbl homodimers were unstable in IFT20-deficient cells, which was evident by the reduction in coprecipitated, GFP-tagged c-Cbl$^{*RING}$ (Fig. 3 h), indicating that IFT20 is also required to promote formation of stable c-Cbl dimers.

To confirm those findings, we tested whether defects in the feedback inhibition of PDGFRα signaling in IFT20-depleted cells could be phenocopied by depletion of Cbl proteins. We performed siRNA knockdown experiments in WT NIH3T3 cells and examined activation of PDGFRα and AKT upon PDGF-AA stimulation in serum-starved cells. Interestingly, a significant increase and prolongation of PDGFRα signaling was only detected in cells depleted for both c-Cbl and Cbl-b (Fig. 3, i and j), which is consistent with our findings in IFT20-deficient cells (Fig. 1, g–i). To our knowledge, this result demonstrates for the first time that removal of both Cbl ubiquitin ligases is required for efficient down-regulation of PDGFRα signaling.

## IFT20 interacts with Cbl proteins, and c-Cbl is targeted to the cilium upon PDGF-AA stimulation

Because IFT20 is required for stability and function of c-Cbl and Cbl-b, we then asked whether those proteins interact physically with IFT20. We initially evaluated such an interaction with

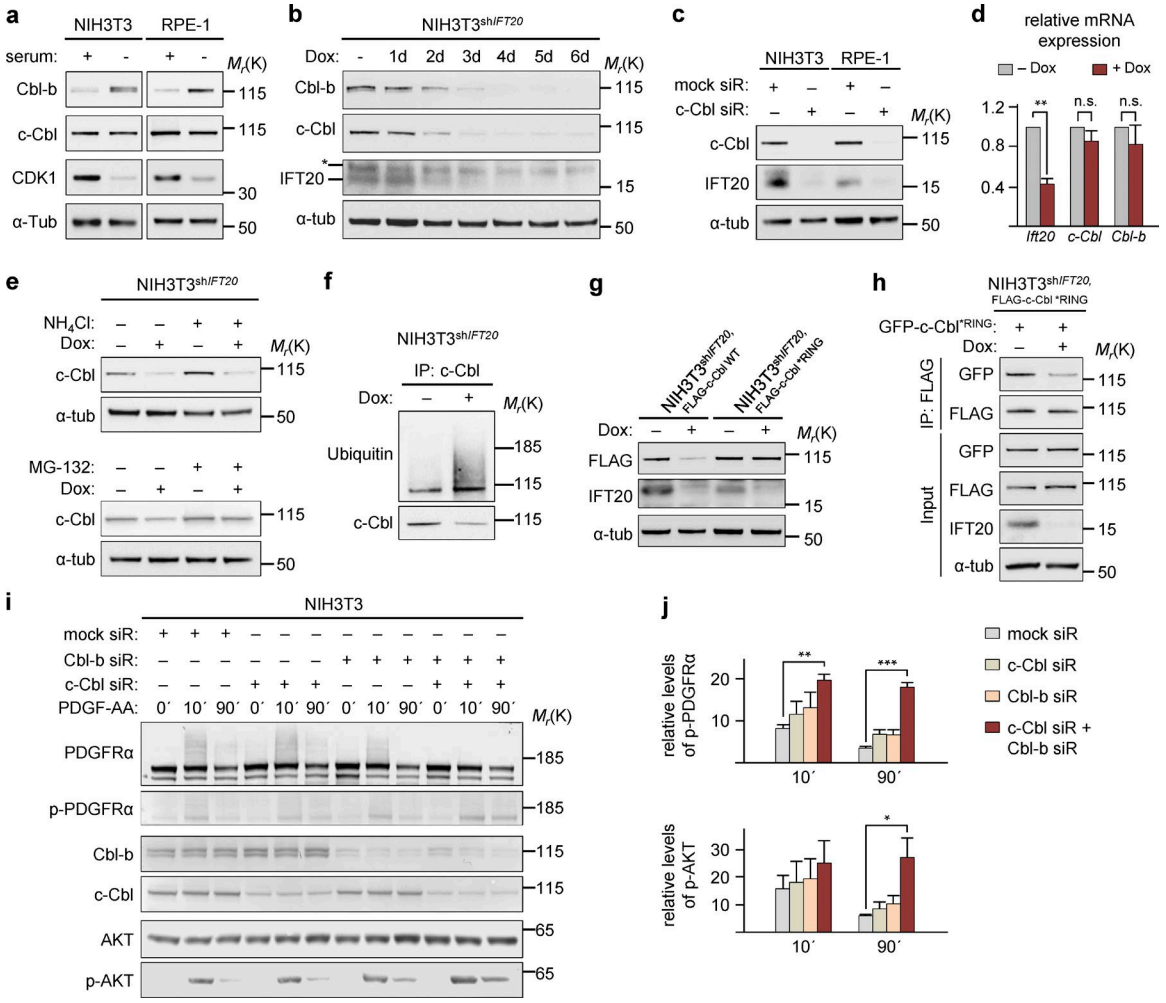


Figure 3. **Cbl family E3 ubiquitin ligases are degraded in cells with reduced IFT20, leading to defects in termination of PDGFRα signaling. (a)** WB analysis showing expression levels of c-Cbl and Cbl-b proteins in cycling (+ serum) and growth-arrested (– serum) NIH3T3 and RPE-1 cells. CDK1 marks cycling cells. **(b)** WB analysis of c-Cbl and Cbl-b in growth-arrested NIH3T3$^{shIFT20}$ cells upon addition of Dox for 1–6 d. All cells were grown for 6 d, including 24 h of serum depletion before analysis. An unspecific band stained by the IFT20 antibody is labeled with an asterisk. **(c)** WB analysis of IFT20 in growth-arrested NIH3T3 and RPE-1 cells subjected to mock or siRNA(siR)-mediated silencing of c-Cbl. **(d)** Quantitative, real-time PCR analysis of relative *Ift20*, *c-Cbl*, and *Cbl-b* mRNA transcript levels in NIH3T3$^{shIFT20}$ upon 6 d of Dox treatment, including 24 h of serum depletion. Error bars represent means ± SEM ($n$ = 3). **(e)** WB analysis of c-Cbl and Cbl-b in cycling NIH3T3$^{shIFT20}$ cells upon Dox treatment for 3 d in combination with lysosomal ($NH_4Cl$) or proteasomal (MG-132) inhibitors for 24 h or 10 h, respectively. **(f)** IP of endogenous c-Cbl in NIH3T3$^{shIFT20}$ cells with or without Dox for 3 d, followed by WB analysis with antibodies against mono- and polyubiquitin. **(g)** WB analysis of growth-arrested NIH3T3$^{shIFT20}$ cells stably expressing FLAG–tagged WT or RING-mutant c-Cbl (NIH3T3$^{shIFT20,FLAG–c-Cbl,WT}$ and NIH3T3$^{shIFT20,FLAG–c-Cbl*RING}$, respectively) upon 6 d of Dox treatment. **(h)** FLAG IP of protein lysates from NIH3T3$^{shIFT20,FLAG–c-Cbl*RING}$ cells transiently expressing GFP-tagged c-Cbl RING mutant (GFP-c-Cbl$^{*RING}$) after treatment with Dox for 4 d. Experiments presented in panels a–c and e–h were repeated at least three times, and results from representative experiments are shown. **(i)** WB analysis of phosphorylation of PDGFRα (p-PDGFRα) and AKT (p-AKT) upon stimulation with 50 ng/ml PDGF-AA for indicated times in NIH3T3 cells subjected to siRNA (siR)-mediated silencing of c-Cbl, Cbl-b, or both for 72 h, including serum depletion for the last 24 h before stimulation to induce growth arrest. **(j)** Quantification of protein phosphorylations shown in panel i. Error bars represent means ± SEM ($n$ = 3).

a FLAG–IFT20 IP assay in HEK293T-cell extracts and mass spectrometric analysis of coprecipitated immunocomplexes. We found c-Cbl to coprecipitate with FLAG–IFT20 (Fig. S3 a and Table S1), and that interaction was confirmed by IP of FLAG-tagged c-Cbl (FLAG–c-Cbl$^{WT}$) when GFP-tagged IFT20 was co-precipitated (Fig. 4 a). Supportively, IP of endogenous proteins demonstrated binding of c-Cbl to IFT20 and vice versa (Fig. 4, b and c), suggesting that those proteins interact physically. Because heterodimerization of c-Cbl and Cbl-b relies on their C-terminal ubiquitin-associated/leucine zipper domains (Liu et al., 2003; Rorsman et al., 2016), we further asked whether Cbl-b might participate in an IFT20–c-Cbl complex. Initially, we found that Cbl-b was immunoprecipitated with FLAG–c-Cbl$^{WT}$ as well as with a defective form of ubiquitin ligase carrying the mutation p.C381A in the RING-finger domain of c-Cbl (Waterman et al., 1999; FLAG–c-Cbl$^{*RING}$; Fig. 4 d), indicating that the interaction between c-Cbl and Cbl-b was independent of ubiquitin ligase activity. Indeed, reciprocal IFT20 pulldown of cell extracts from FLAG–c-Cbl expressing cells coprecipitated both endogenous Cbl-b and FLAG–c-Cbl. Interestingly, although the protein levels of IFT20 in those cells remained unchanged, IFT20 appeared to bind more avidly to RING-mutated FLAG–c-Cbl and Cbl-b than it did with WT FLAG–c-Cbl (Fig. 4 e). Despite those findings, size-exclusion chromatography of extracts from HEK293T cells revealed only a minor overlap between the elution profile of IFT20 and those of c-Cbl and Cbl-b (Fig. S3 b), suggesting that

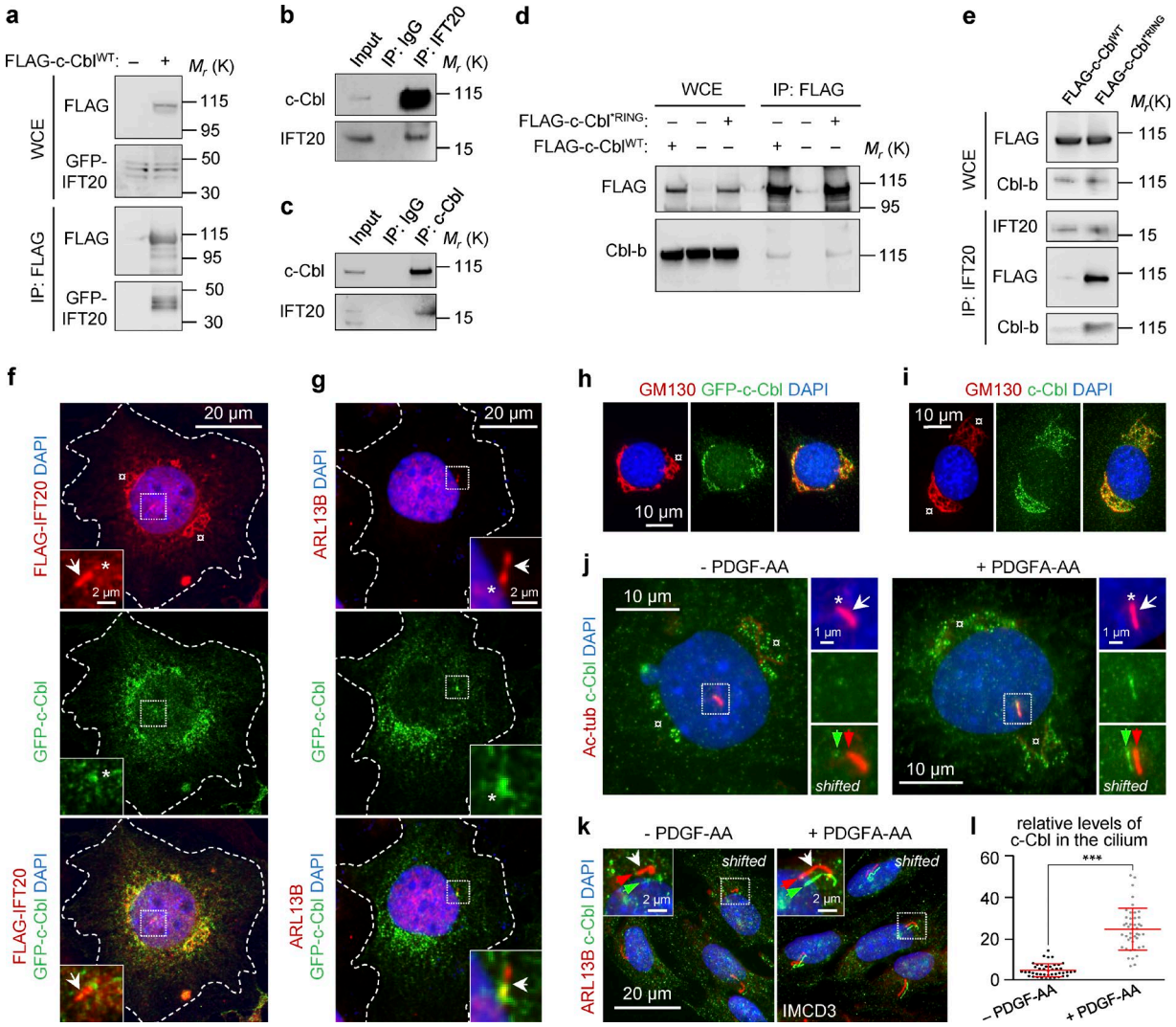


Figure 4. **IFT20 interacts with Cbl-b and c-Cbl, which is targeted to the cilium in PDGF-AA–stimulated cells. (a)** Validation of the IFT20-c-Cbl interaction. HEK293T cells coexpressing GFP-IFT20 with either FLAG–tagged WT c-Cbl (FLAG–c-Cbl$^{WT}$) or empty FLAG vector were subjected to FLAG IP, followed by WB analysis. **(b and c)** Reciprocal IPs of endogenous IFT20 or c-Cbl from HEK293T cells. **(d)** FLAG IP of HEK293T cell extracts expressing FLAG–c-Cbl$^{WT}$ or FLAG–tagged RING mutant (p.C381A) c-Cbl (FLAG–c-Cbl$^{*RING}$). **(e)** IFT20 IP of HEK293T cell extracts expressing FLAG–c-Cbl$^{WT}$ or FLAG–c-Cbl$^{*RING}$, followed by WB analysis. **(f)** IFM of WT NIH3T3 cells coexpressing GFP-tagged c-Cbl and FLAG–tagged IFT20. The dashed line indicates the Golgi complex, the arrow shows the primary cilium, and the asterisks identify the ciliary base. The nucleus was visualized with DAPI. **(g)** IFM of WT NIH3T3 cells expressing GFP-tagged c-Cbl. The primary cilium was marked with anti–ARL13B (arrow). The dashed line indicates the Golgi complex, and asterisk indicates the ciliary base. The nucleus was visualized with DAPI. The outline of the cells in panels f and g is highlighted with a dashed line. **(h and i)** IFM of WT NIH3T3 cells expressing either GFP-tagged c-Cbl (h) or stained with anti–c-Cbl (i). The Golgi complex (dashed line) was labeled with anti–GM130, and the nucleus was visualized with DAPI. **(j)** Localization of c-Cbl to the primary cilium in WT NIH3T3 cells, labeled with anti–Ac-tub (arrow), in WT NIH3T3 cells before and after stimulation with PDGF-AA. The asterisk marks the ciliary base. The nucleus was visualized with DAPI. **(k)** Localization of c-Cbl to the primary cilium in WT NIH3T3 cells and labeled with anti–ARL13B (arrow) in IMCD3 cells before and after stimulation with PDGF-AA. The asterisk marks the ciliary base. The nucleus was visualized with DAPI. **(l)** Quantification of relative levels of c-Cbl in the primary cilium shown in panel k. Fluorescence was normalized to background levels. For each of the three experiments, >15 cells were quantified. Error bars represent means ± SEM ($n$ = 3).

only a fraction of the cellular IFT20 was complexed with the Cbl proteins. This is not surprising given that IFT20 is an integral component of the IFT-B subcomplex (Cole et al., 1998; Taschner et al., 2016). Collectively, these results suggest that only a portion of cellular IFT20 interacts physically with both c-Cbl and Cbl-b and that the interaction between IFT20 and Cbl-b may, in part, be mediated through binding to c-Cbl, although that conjecture requires further examination.

To investigate whether a link exists between IFT20 interaction and the function of Cbl proteins in the primary cilium, we monitored the localization of c-Cbl in the presence and in the absence of PDGF-AA in ciliated WT NIH3T3 and inner medullary collecting duct 3 (IMCD3) cells by IFM analysis. Initially, GFP-tagged c-Cbl was shown to localize predominantly at the base and the proximal part of the primary cilium as well as in the Golgi complex in unstimulated NIH3T3 cells (Fig. 4, f–i). After 10 min of PDGF-AA stimulation, endogenous c-Cbl was enriched in the primary cilium, whereas Golgi localization was largely unaffected (Fig. 4, j–l). Based on those observations, we suggest that the Golgi complex and the ciliary-base region are potential compartments for interaction between IFT20 and Cbl proteins and that the Cbl proteins are recruited to the cilium to initiate feedback inhibition of activated PDGFRα.

### PDGFRα mislocalizes to the plasma membrane in cells with reduced IFT20 and Cbl proteins

Because PDGFRα is labeled at the cell surface (Fig. 2 b) and is capable of being activated by PDGF-AA in IFT20-depleted cells (Fig. 1, g and h), we inferred that the receptor under those circumstances was aberrantly localized to the cell surface outside the primary cilium. To confirm that hypothesis, we generated NIH3T3$^{shIFT20}$ cells that stably expressed GFP-tagged PDGFRα (NIH3T3$^{shIFT20,GFP–PDGFRα}$; Fig. 5, a and b) and subjected those cells to Dox treatment. In growth-arrested, untreated cells, the GFP-tagged receptor localized to the primary cilium, in the Golgi, and at the perinuclear region surrounding the Golgi complex (Fig. 5, a and c), as previously described for RPE-1 cells (Nielsen et al., 2015). In contrast, GFP–PDGFRα localization was more dispersed throughout the cytosol in IFT20-deficient cells, with part of the receptor population localizing at the plasma membrane and often to patches at that site (Fig. 5, a and e). Similar results were obtained for endogenous PDGFRα in NIH3T3$^{shIFT20}$ cells (Fig. 5 d), whereas in WT NIH3T3 cells treated with Dox, the receptor was undetectable at the plasma membrane (Fig. S3 c). Quantification of GFP–PDGFRα fluorescence intensity, in a 5-µm region spanning from the cell surface into the cell, revealed significantly more of the receptor close to the cell surface (Fig. 5, e and f). Similarly, GFP-tagged PDGFRα was also enriched at the lamellipodium of migrating cells deficient for IFT20 (Fig. 5 g), indicating that localization of the receptor to the plasma membrane in the absence of IFT20 is linked to cell polarity. Because IFT20 stabilizes c-Cbl and Cbl-b to modulate PDGFRα signaling, we further investigated the localization of the receptor in NIH3T3$^{shIFT20,GFP–PDGFRα}$ cells subjected to siRNA-mediated knockdown of both Cbl proteins. Under those conditions, GFP-tagged PDGFRα was similarly localized toward the plasma membrane (Fig. 5 h) and prominently confined in puncta along extensive cellular protrusions (Fig. S3 d). These results underscore the functional relationship between IFT20 and Cbl proteins in receptor sorting and modulation of PDGFRα signaling.

Our results support the conclusion that defects in IFT proteins and ciliary trafficking affect PDGFRα signaling by different mechanisms. In contrast to IFT20 depletion, fibroblasts lacking IFT88 and IFT172 have reduced PDGFRα expression, and the receptor cannot be activated by stimulation with PDGF-AA (Schneider et al., 2005; Umberger and Caspary, 2015). There are several possibilities to explain those differences. Based on our findings, one model would be that IFT20 in collaboration with c-Cbl and Cbl-b ensures targeting of PDGFRα from the Golgi complex to the cilium and, at the same time, impedes localization in the plasma membrane. Whether trafficking from the Golgi complex to the cilium follows a direct pathway or is regulated via recycling endosomes from the plasma membrane, as shown for polycystin-2 (Monis et al., 2017), remains unknown. Upon PDGF-AA binding to the receptor, Cbl proteins accumulate in the primary cilium to coordinate the processes of receptor ubiquitination and internalization for balanced feedback inhibition of PDGFRα signaling (Fig. 5 i). However, further investigations are required to understand whether that accumulation is caused by changes in the rate of ciliary entry or the rate of ciliary exit of the proteins and whether ciliary accumulation is regulated by interaction with IFT20 or by other proteins in the cilium proper. In particular, IFT20 appears to be especially important for complex integrity because depletion of IFT20, but not IFT88 or IFT172, results in degradation of both Cbl proteins, whereas depletion of one of the Cbl proteins alone seems to have little effect on the stability of the other paralog. In support of that understanding, only codepletion of c-Cbl and Cbl-b caused overactivation of PDGFRα signaling and receptor localization to the plasma membrane, thus phenocopying IFT20 knockdown and underscoring the importance of IFT20 for maintenance of the stability and function of Cbl proteins. Interestingly, fibroblasts deficient in the IFT-A subcomplex protein IFT122, which display swollen or bulgy cilia because of defective, retrograde IFT (Ocbina et al., 2011), show normal levels of PDGFRα, which can be activated by short term stimulation with PDGF-AA (Umberger and Caspary, 2015), indicating that the receptor in those cells is targeted to the cilium for activation. However, because IFT122 has been shown to regulate the balanced output of cellular signaling through the coordinated trafficking of signaling constituents out of the cilium, such as in Hedgehog signaling (Qin et al., 2011), we surmise that feedback inhibition PDGFRα signaling in IFT122-deficient fibroblasts could be affected in IFT122-deficient cells, although that is speculative at this point.

Finally, it will be important to investigate whether the interaction between IFT20 and Cbl proteins also occurs in cell types other than fibroblasts and whether such interplay is disrupted in disease. IFT20 governs clustering of a functional TCR/CD3 complex containing LAT at the immune synapse in T cells (Finetti et al., 2009, 2014; Vivar et al., 2016), and Cbl proteins also have important roles in TCR turnover, and mutations in c-Cbl cause leukemia and autoimmune diseases (Liyasova et al., 2015). In a recent study, osteoblasts derived from IFT20 knockout mice embryos were shown to display mildly reduced AKT phosphorylation in response to short term stimulation with PDGF-AA (Noda et al., 2016). Although that study did not address the role of IFT20 in modulation of feedback inhibition of PDGFRα signaling during long-term stimulation with PDGF-AA, there might be cell type–specific differences or adaptations because of the long-lasting lack of IFT20 and Cbl proteins in mutant osteoblasts. Thus, investigating Cbl proteins in that context would be very informative toward elucidating how cells compensate to survive those deleterious effects and become tumorigenic. Indeed, aberrant PDGFRα signaling has been linked to a broad range of human pathologies, such as gastrointestinal stromal tumors (Andrae et al., 2008; Corless et al., 2011) and glioblastoma (Heldin and Lennartsson, 2013), and defects in Cbl proteins account for the pathogenesis of leukemia and autoimmune diseases (Liyasova et al., 2015). Likewise, defects in the function of primary cilia have been associated with tumorigenesis and cancer (Seeger-Nukpezah et al., 2013).

## Materials and methods

#### Reagents

The following antibodies were used: R&D Systems: goat anti-PDGFRα (AF1062); Proteintech: rabbit anti–human IFT20 (13615–1-AP), rabbit anti-IFT88 (13967-1-AP); Sigma-Aldrich: mouse anti–α-tubulin (T5168), mouse anti–acetylated α-tubulin (T6793), mouse anti-FLAG (M2; F1802), rabbit anti-FLAG (F7425); BD Biosciences: mouse anti-CDK1 (610038), mouse anti-p150$^{Glued}$ (610474), mouse anti-GM130 (610823); Enzo life Sciences: mouse anti-giantin (ALX-804-600-C100), mouse anti–mono- and polyubiquitin (FK2; BML-PW8810); Abcam: mouse anti–c-Cbl (Ab119954), rabbit anti–c-Cbl (Ab32027), mouse

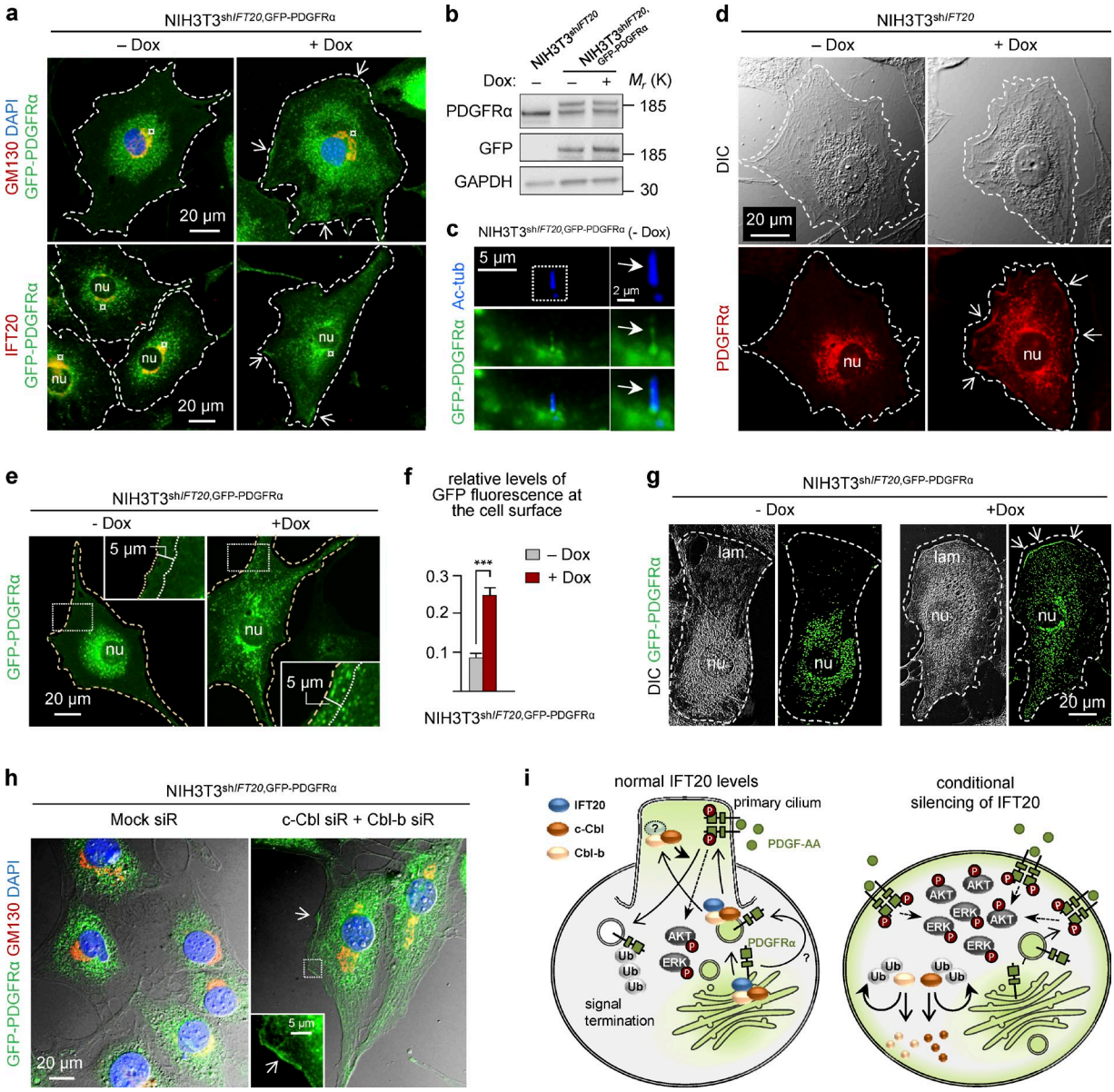


Figure 5. **PDGFRα localizes at the plasma membrane in IFT20-depleted cells.** In all experiments, cells were incubated with or without Dox for 6 d, including serum depletion for 24 h before analysis. **(a)** IFM of NIH3T3$^{shIFT20}$ cells expressing GFP-tagged PDGFRα (NIH3T3$^{shIFT20,GFP\text{-}PDGFR\alpha}$) stained with anti–IFT20 and anti–GM130 to label the Golgi complex (dashed line). Nuclei (Nu) were visualized with DAPI. Arrows indicate receptor localization at the plasma membrane. The outline of the cells is highlighted by a dashed line. **(b)** WB analysis of PDGFRα and GFP-PDGFRα in NIH3T3$^{shIFT20}$ and NIH3T3$^{shIFT20,GFP\text{-}PDGFR\alpha}$ with or without Dox. GAPDH was used as the loading control. **(c)** IFM showing localization of GFP–PDGFRα to the primary cilium (arrow) labeled with anti–Ac-tub in the absence of Dox. **(d)** IFM of localization of endogenous PDGFRα in NIH3T3$^{shIFT20}$ cells with or without Dox. Nuclei (Nu) were visualized with DIC microscopy. Arrows indicate receptor localization at the plasma membrane. **(e and f)** Relative levels of GFP fluorescence at the cell surface in NIH3T3$^{shIFT20,GFP\text{-}PDGFR\alpha}$ cells, corresponding to a 5-μm area starting from the cell surface into the inside of the cell (e). GFP fluorescence was normalized to background levels. For each of 3 experiment, >15 cells were quantified. Error bars represent SEM ($n$ = 3; f). **(g)** IFM analysis of GFP-PDGFRα localization in migrating NIH3T3$^{shIFT20,GFP\text{-}PDGFR\alpha}$ cells with or without Dox. Arrows indicate localization of receptors to the leading-edge membrane of the lamellipodia (lam.) in cells treated with Dox. **(h)** IFM analysis of GFP-PDGFRα localization in NIH3T3$^{shIFT20,GFP\text{-}PDGFR\alpha}$ cells subjected to siRNA-mediated silencing of both c-Cbl and Cbl-b. GM130 labels the Golgi complex. Arrows indicate localization of receptors at the plasma membrane (h) and to cellular protrusions in cells treated with Dox. Nuclei were visualized with DAPI. **(i)** Proposed model for the role of IFT20 in modulating PDGFRα signaling. IFT20 interacts with c-Cbl and Cbl-b to orchestrate the ubiquitination and internalization of ligand-activated PDGFRα for signaling termination. In the presence of IFT20 (left), PDGFRα is activated with proper feedback inhibition at the primary cilium, but in IFT20-depleted cells with defective ciliogenesis (right), PDGFRα mislocalizes to the plasma membrane from where the receptor is overactivated because of autoubiquitination-induced degradation of c-Cbl and Cbl-b.

anti-GFP (Ab1218), chicken anti-GFP (Ab13970), rabbit anti–detyrosinated α-tubulin (Ab48389), rabbit anti-PDGFRα (Ab134123); Cell Signaling Technology: rabbit anti-Myc (2278), rabbit anti-GAPDH (2118), rabbit anti–Cbl-b (9498), rabbit anti-Akt (9272), rabbit anti–phosphorylated Akt (Ser473; 4060), rabbit anti-Erk1/2 (9102), rabbit anti–phosphorylated Erk1/2 (Thr202/Tyr204; 9101), rabbit anti–phosphorylated Rb (9308); Santa Cruz Biotechnology: rabbit anti–c-Cblsc-170), mouse anti–c-Cbl (sc-1651), mouse anti-GFP (sc-9996), rabbit anti-GFP (sc-8334), rabbit anti–phosphorylated PDGFRα (Tyr754; sc-12911R). For RNAi-mediated gene-silencing experiments, custom siRNAs were purchased from Eurofins Genomics. The siRNA sequences 5′-UAAUGUAUUGGAAGGCAUA-3′ or 5′-CCAACG

ACCUGGAGAUUAA-3′ were used for mock or for gene silencing of mouse IFT88, respectively. Sequences of other siRNAs used in this manuscript have been described elsewhere: siRNA against human (Selbach and Mann, 2006) and mouse (Mitra et al., 2004) c-Cbl, and siRNA against mouse Cbl-b (Hinterleitner et al., 2012). Cells were transfected at a concentration of 300 nM of total siRNA and incubated for 72 h to induce an efficient mRNA silencing. Recombinant PDGF-AA (at 50 ng/ml) was purchased from R&D Systems. Cells were treated with the following chemicals: MG-132 (10 µM for 10 h; Selleck Chemicals), $NH_4Cl$ (10 mM for 24 h; Sigma-Aldrich), and Dox (0.5 µg/ml for 3, 4, or 6 d; Sigma-Aldrich). If not otherwise stated, concentration and incubation times indicated in brackets have been applied.

### Plasmid constructs

For plasmid constructs inducibly expressing shRNA against human and mouse IFT20, DNA sequences previously described (Follit et al., 2006) were cloned into pSuperior (Oligoengine), following the manufacturer's protocol. For the construct expressing GFP-tagged, siRNA-resistant IFT20 (pJAF2.13-Res), pJAF2.13 (Follit et al., 2006; provided by G. Pazour, University of Massachusetts Medical School, Worcester, MA) was mutated using Agilent's QuickChange II site-directed mutagenesis kit and mutant primers. A construct expressing C-terminal–GFP-tagged PDGFRα was used for stable expression in NIH3T3$^{shIFT20}$ cells and was generated in two steps, by first, transferring the GFP-coding sequence from pEGFP-N1 (Clontech) into pcDNA5/FRT (Life Technologies) using HindIII and NotI restriction sites to get pcDNA5/FRT-GFP. In the second step, PDGFRα-coding sequence was cloned from PDGFRα WT-GFP into pcDNA5/FRT-GFP using HindIII and KpnI. Cloning of PDGFRα WT-GFP has been described previously (Nielsen et al., 2015). Plasmid expressing human c-Cbl was purchased from Origene (RC214069). To generate c-Cbl *RING FLAG, the ubiquitin ligase–inactivating mutation p.C381A (Joazeiro et al., 1999; Waterman et al., 1999) was introduced by standard PCR using mutant primers and the same flanking primers as used to generate c-Cbl WT FLAG. Truncated versions of c-Cbl were produced by standard PCR on c-Cbl WT FLAG using specific, reverse primers that bind to C-terminal ends of selected protein-binding domains of c-Cbl and by using the same forward primer. The construct expressing the GFP-tagged c-Cbl RING mutant (c-Cbl *RING GFP) was obtained by cloning the c-Cbl coding sequence from c-Cbl *RING FLAG into pEGFP-N1. Plasmid expressing Myc-tagged ubiquitin was a gift from J. Bartek at the Danish Cancer Society (Copenhagen, Denmark). Correct sequences for all constructs were verified by Sanger sequencing using the sequencing service from Eurofins Genomics.

### Mammalian cell culture, transfection, and generation of stable cell lines

HEK293, NIH3T3, IMCD3, and RPE-1 cells were grown in DMEM (Life Technologies), supplied with 10% FBS and 1% penicillin/streptomycin (Gibco). If not otherwise stated, ciliogenesis was induced by serum depletion for 24 h. For transfection with siRNA or plasmid DNA constructs, DharmaFECT Duo (Dharmacon) or FuGENE 6 (Promega) were used, respectively, by following manufacturers' protocols. To generate the NIH3T3$^{shIFT20}$ cell line for Dox-inducible depletion of IFT20, pSuperior (Oligoengine) containing shRNA targeting mouse IFT20 was cotransfected with pcDNA6/TR (Life Technologies) following the manufacturer's instructions. Cells stably expressing both constructs were selected with 5 µg/ml puromycin (Gibco) and 10 µg/ml blasticidin (Life Technologies). Cell lines NIH3T3$^{shIFT20,shIFT20\text{-Res}}$, NIH3T3$^{shIFT20,GFP\text{-}PDGFR\alpha}$, NIH3T3$^{shIFT20,FLAG\text{–}c\text{-}Cbl,WT}$, and NIH3T3$^{shIFT20,\text{-}FLAG\text{–}c\text{-}Cbl*RING}$ were generated by transfection of NIH3T3$^{shIFT20}$ cells with pJAF2.13-Res, PDGFRα WT-GFP, FLAG–c-Cbl$^{WT}$, or FLAG–c-Cbl$^{*RING}$, respectively. In addition to selection with puromycin and blasticidin, NIH3T3shIFT20,$^{GFP\text{-}PDGFR\alpha}$, NIH3T3$^{shIFT20,FLAG\text{–}c\text{-}Cbl,WT}$, and NIH3T3$^{shIFT20,FLAG\text{–}c\text{-}Cbl*RING}$ cell lines were grown in 30 µg/ml Hygromycin B (Life Technologies), whereas NIH3T3$^{shIFT20,shIFT20\text{-Res}}$ was grown in 800 µg/ml G418 (Sigma-Aldrich).

### Immunofluorescence, microscopic analysis, and quantification of GFP fluorescence

Cells were grown on glass coverslips and fixed in either 4% PFA or 100% methanol for 15 min at RT or 10 min at −20°C, respectively. For PFA fixed cells, cell membranes were permeabilized by incubation in 1× PBS, 1% BSA, and 0.2% Triton X-100 for 12 min at RT. Thereafter, cells were incubated in 1× PBS and 2% BSA for 30 min at RT to block unspecific binding of antibodies, followed by overnight incubation with primary antibodies at 4°C. After PBS washing steps, cells were incubated in corresponding Alexa Fluor–conjugated secondary antibodies (Invitrogen) for 45 min at RT. Cell nuclei were labeled by DAPI staining or detected through differential interference contrast (DIC) microscopy. Coverslips were mounted in 1× PBS, 90% glycerol, and 2% *N*-propyl-gallate on glass slides and sealed with nail polish. Images were captured on a fully motorized BX63 upright microscope (Olympus) with a DP72 color, 12.8-megapixel, 4,140 × 3,096–resolution camera, and DIC. For quantification of receptor localization, the mean fluorescence value of GFP-PDGFRα at a region comprising a 5-µm area, starting from the cell surface into the inside of the cell, was set relative to the fluorescence value of the entire cell. For quantification of c-Cbl fluorescence in the primary cilium, values in the cilium region were set relative to the fluorescence values in background areas of the cytosol.

### Quantitative, real-time PCR

Total RNA was extracted from cells with Nucleospin RNA II kit (Macherey-Nagel) following the manufacturer's protocol. 1 µg of total RNA was reverse-transcribed into cDNA using SuperScript III reverse transcription (Life Technologies). The quantitative, real-time PCR reactions were performed on a 7500 Fast Real-Time PCR system from Applied Biosystems with Lightcycler Fast Start DNA Master plus SYBR Green I (Roche). Transcript levels of genes of interest were normalized to transcript levels of housekeeping genes *GAPDH*, *HRP*, and *PSMD4*, and means were obtained.

### Cell lysis, IP, SDS PAGE, and WB analysis

Total protein was extracted by cell lysis in SDS (10 mM Tris-HCl and 1% SDS), EBC buffer (140 mM NaCl, 50 mM Tris-HCl, 1 mM Na3VO4, 5 mM EDTA, and 0.5% NP-40), or CHAPS buffer (20 mM Tris, 20 mM NaCl, 1 mM EDTA, 5 mM EGTA, 1 mM dithiothreitol, and 0.1% CHAPS, pH 7.4) plus protease inhibitor cocktail (Roche), followed by clearing of cell lysates through centrifugation at 20.000 *g* for 30 min. For IP assays, anti-FLAG (M2) antibody–conjugated agarose beads or protein A– or G–conjugated sepharose beads (Sigma-Aldrich) in combination with their corresponding antibodies were used, following the manufacturer's instructions. Proteins were eluted from five-time prewashed immunocomplexes using 2× LDS sample buffer (IPs for ubiquitination and dimerization experiments; Life Technologies), 0.2 mM glycine, pH 2.5 (IPs for protein interaction studies), or 3× FLAG peptide (IP for mass spectrometry [MS]). SDS-PAGE and WB analysis with corresponding antibodies was performed as previously described (Schrøder et al., 2011; Nielsen et al., 2015). Membranes were incubated with secondary antibodies conjugated with either alkaline phosphatase or HRP and developed with BCIP/NBT (Kem-En-Tec Diagnostics) and ECL Western Blotting Detection Reagents (GE Healthcare Life Sciences), respectively. Band intensities from blots

obtained with colorimetric substrate (scanned blots) and chemiluminescence were estimated from arbitrary densitometric values obtained with UN-SCAN-IT version 5.1 software (Silk Scientific, Inc.). Blots were further processed for publication with Photoshop version CS6 (Adobe) using the Level function for contrast adjustment. Processing was applied equally across the entire blot and equally to controls.

### Size-exclusion chromatography

Native protein complexes from HEK293T cells were run by HPLC on an $NaPO_4$-buffered Superose 6 column 10/300 GL (GE Healthcare Life Sciences), and collected fractions were concentrated by vacuum centrifugation.

### MS

SDS-PAGE–resolved, 4–12%-gradient gels were silver-stained with SilverQuest (Life Technologies), and appropriate bands were cut and subjected to in-gel digestion, followed by liquid chromatography–MS with a Q Exactive HF system (Thermo Fisher Scientific). Resulting peptides were identified by protein-sequence database searches using MaxQuant software.

### Biotinylation assays

Cell surface proteins were labeled with biotin by incubation of cells in 1× PBS containing 0.25 mg/ml EZ-Link Sulfo-NHS-SS-Biotin for 30 min on ice. To detect localization of PDGFRα specifically at the cell surface upon ligand addition, cells were stimulated with 50 ng/ml PDGF-AA for the indicated times before biotin labeling. To detect internalized PDGFRα, cells were stimulated after labeling with biotin, and biotinylation of proteins at the cell surface was removed by treatment with glutathione-stripping solution (50 mM reduced glutathione, 150 mM NaCl, 70 mM NaOH, 1.25 mM $MgSO_4$, 1.25 mM $CaCl_2$, and 1 mM EDTA, pH 8.5) for 10 min on ice. For total amounts of biotinylated PDGFRα receptor, the same procedure was applied, except for stripping of biotin from cell surface proteins. SDS-PAGE and WB analyses were performed with the rabbit anti–PDGFRα antibody (Abcam).

### Statistical analysis

Statistical analyses represent the means of at least three independent experiments. Error bars represent standard errors of the mean (SEM; $n = 3$). P-values were calculated using the Student's $t$ test, if not specified: *, $P < 0.05$; **, $P < 0.01$; ***, $P < 0.001$; n.s., not significant.

### Online supplemental material

Fig. S1 shows that Dox treatment itself does not affect PDGFRα signaling in WT NIH3T3 cells and that PDGFRα is up-regulated at the protein level in growth-arrested cells depleted for IFT20. Fig. S2 shows the functional and biochemical interdependence of IFT20 and c-Cbl on the protein level and that the effect of IFT20 depletion on Cbl stabilization is not solely a consequence of ciliary loss. Fig. S3 shows that IFT20, c-Cbl, and Cbl-b interact as indicated by MS and size-exclusion chromatography; that Dox treatment itself does not affect PDGFRα localization to the plasma membrane; and that codepletion of c-Cbl and Cbl-b leads to localization of GFP-tagged PDGFRα to the plasma membrane and prominently confined in puncta along extensive cellular protrusions. Table S1 shows MS–based analysis of proteins interacting with FLAG–IFT20.

## Acknowledgments

We thank Søren Lek Johansen and Lillian Rasmussen for excellent technical assistance and we are grateful to G. Pazour for reagents.

This study was supported by the Lundbeck Foundation (grants R54-A5375 and R54-A5642), the Independent Research Fund Denmark (grants 09-070398, 10-085373, 1331-00254, and 6108-00457B), the Danish Cancer Society (grant R56-A3151-12-S2), the Novo Nordisk UK Research Foundation (grants NNF14OC0011535 and NNF15OC0016886), the Carlsberg Foundation, and the University of Copenhagen Excellence Program for Interdisciplinary Research. F.M. Schmid was supported by Schweizerischer Nationalfonds zur Förderung der Wissenschaftlichen Forschung and Velux Stiftung fellowships.

The authors declare no competing financial interests.

Author contributions: S.T. Christensen, F.M. Schmid, K.B. Schou, and L.B. Pedersen designed the research. F.M. Schmid, K.B. Schou, M.J. Vilhelm, M.S. Holm, L. Breslin, P. Farinelli, L.A. Larsen, J. Andersen, and S.T. Christensen performed the experiments. All authors analyzed and discussed the data. S.T. Christensen, F.M. Schmid, and K.B. Schou wrote the paper. All co-authors reviewed and edited the paper. S.T. Christensen, L.B. Pedersen, L.A. Larsen, and J.S. Andersen obtained funding for the study.

Submitted: 8 November 2016
Revised: 20 January 2017
Accepted: 24 August 2017

## References

Andrae, J., R. Gallini, and C. Betsholtz. 2008. Role of platelet-derived growth factors in physiology and medicine. *Genes Dev.* 22:1276–1312. https://doi.org/10.1101/gad.1653708

Bonita, D.P., S. Miyake, M.L. Lupher Jr., W.Y. Langdon, and H. Band. 1997. Phosphotyrosine binding domain-dependent upregulation of the platelet-derived growth factor receptor alpha signaling cascade by transforming mutants of Cbl: implications for Cbl's function and oncogenicity. *Mol. Cell. Biol.* 17:4597–4610. https://doi.org/10.1128/MCB.17.8.4597

Christensen, S.T., S.K. Morthorst, J.B. Mogensen, and L.B. Pedersen. 2017. Primary cilia and coordination of receptor tyrosine kinase (RTK) and transforming growth factor beta (TGF-β) signaling. *Cold Spring Harb. Perspect. Biol.* 9:a028167. https://doi.org/10.1101/cshperspect.a028167

Clement, D.L., S. Mally, C. Stock, M. Lethan, P. Satir, A. Schwab, S.F. Pedersen, and S.T. Christensen. 2013. PDGFRα signaling in the primary cilium regulates NHE1-dependent fibroblast migration via coordinated differential activity of MEK1/2-ERK1/2-p90RSK and AKT signaling pathways. *J. Cell Sci.* 126:953–965. https://doi.org/10.1242/jcs.116426

Coats, S.R., H.D. Love, and W.J. Pledger. 1994. Platelet-derived growth factor (PDGF)-AB-mediated phosphorylation of PDGF beta receptors. *Biochem. J.* 297:379–384. https://doi.org/10.1042/bj2970379

Cole, D.G., D.R. Diener, A.L. Himelblau, P.L. Beech, J.C. Fuster, and J.L. Rosenbaum. 1998. *Chlamydomonas* kinesin-II–dependent intraflagellar transport (IFT): IFT particles contain proteins required for ciliary assembly in *Caenorhabditis elegans* sensory neurons. *J. Cell Biol.* 141:993–1008. https://doi.org/10.1083/jcb.141.4.993

Corless, C.L., C.M. Barnett, and M.C. Heinrich. 2011. Gastrointestinal stromal tumours: origin and molecular oncology. *Nat. Rev. Cancer.* 11:865–878. https://doi.org/10.1038/nrc3143

Demoulin, J.B., and A. Essaghir. 2014. PDGF receptor signaling networks in normal and cancer cells. *Cytokine Growth Factor Rev.* 25:273–283. https://doi.org/10.1016/j.cytogfr.2014.03.003

Demoulin, J.B., and C.P. Montano-Almendras. 2012. Platelet-derived growth factors and their receptors in normal and malignant hematopoiesis. *Am. J. Blood Res.* 2:44–56.

Farahani, R.M., and M. Xaymardan. 2015. Platelet-Derived Growth Factor Receptor Alpha as a Marker of Mesenchymal Stem Cells in Development and Stem Cell Biology. *Stem Cells Int.* 2015:362753. https://doi.org/10.1155/2015/362753

Finetti, F., S.R. Paccani, M.G. Riparbelli, E. Giacomello, G. Perinetti, G.J. Pazour, J.L. Rosenbaum, and C.T. Baldari. 2009. Intraflagellar transport is required for polarized recycling of the TCR/CD3 complex to the immune synapse. *Nat. Cell Biol.* 11:1332–1339. https://doi.org/10.1038/ncb1977

Finetti, F., L. Patrussi, G. Masi, A. Onnis, D. Galgano, O.M. Lucherini, G.J. Pazour, and C.T. Baldari. 2014. Specific recycling receptors are targeted to the immune synapse by the intraflagellar transport system. *J. Cell Sci.* 127:1924–1937. https://doi.org/10.1242/jcs.139337

Follit, J.A., R.A. Tuft, K.E. Fogarty, and G.J. Pazour. 2006. The intraflagellar transport protein IFT20 is associated with the Golgi complex and is required for cilia assembly. *Mol. Biol. Cell.* 17:3781–3792. https://doi.org/10.1091/mbc.E06-02-0133

Follit, J.A., J.T. San Agustin, F. Xu, J.A. Jonassen, R. Samtani, C.W. Lo, and G.J. Pazour. 2008. The Golgin GMAP210/TRIP11 anchors IFT20 to the Golgi complex. *PLoS Genet.* 4:e1000315. https://doi.org/10.1371/journal.pgen.1000315

Heldin, C.H., and J. Lennartsson. 2013. Structural and functional properties of platelet-derived growth factor and stem cell factor receptors. *Cold Spring Harb. Perspect. Biol.* 5:a009100. https://doi.org/10.1101/cshperspect.a009100

Hinterleitner, R., T. Gruber, C. Pfeifhofer-Obermair, C. Lutz-Nicoladoni, A. Tzankov, M. Schuster, J.M. Penninger, H. Loibner, G. Lametschwandtner, D. Wolf, and G. Baier. 2012. Adoptive transfer of siRNA Cblb-silenced CD8+ T lymphocytes augments tumor vaccine efficacy in a B16 melanoma model. *PLoS One.* 7:e44295. https://doi.org/10.1371/journal.pone.0044295

Joazeiro, C.A., S.S. Wing, H. Huang, J.D. Leverson, T. Hunter, and Y.C. Liu. 1999. The tyrosine kinase negative regulator c-Cbl as a RING-type, E2-dependent ubiquitin-protein ligase. *Science.* 286:309–312. https://doi.org/10.1126/science.286.5438.309

Keady, B.T., Y.Z. Le, and G.J. Pazour. 2011. IFT20 is required for opsin trafficking and photoreceptor outer segment development. *Mol. Biol. Cell.* 22:921–930. https://doi.org/10.1091/mbc.E10-09-0792

Kozlov, G., P. Peschard, B. Zimmerman, T. Lin, T. Moldoveanu, N. Mansur-Azzam, K. Gehring, and M. Park. 2007. Structural basis for UBA-mediated dimerization of c-Cbl ubiquitin ligase. *J. Biol. Chem.* 282:27547–27555. https://doi.org/10.1074/jbc.M703333200

Liu, J., S.M. DeYoung, J.B. Hwang, E.E. O'Leary, and A.R. Saltiel. 2003. The roles of Cbl-b and c-Cbl in insulin-stimulated glucose transport. *J. Biol. Chem.* 278:36754–36762. https://doi.org/10.1074/jbc.M300664200

Liyasova, M.S., K. Ma, and S. Lipkowitz. 2015. Molecular pathways: cbl proteins in tumorigenesis and antitumor immunity-opportunities for cancer treatment. *Clin. Cancer Res.* 21:1789–1794. https://doi.org/10.1158/1078-0432.CCR-13-2490

Mitra, P., X. Zheng, and M.P. Czech. 2004. RNAi-based analysis of CAP, Cbl, and CrkII function in the regulation of GLUT4 by insulin. *J. Biol. Chem.* 279:37431–37435. https://doi.org/10.1074/jbc.C400180200

Miyake, S., M.L. Lupher Jr., B. Druker, and H. Band. 1998. The tyrosine kinase regulator Cbl enhances the ubiquitination and degradation of the platelet-derived growth factor receptor alpha. *Proc. Natl. Acad. Sci. USA.* 95:7927–7932. https://doi.org/10.1073/pnas.95.14.7927

Mohapatra, B., G. Ahmad, S. Nadeau, N. Zutshi, W. An, S. Scheffe, L. Dong, D. Feng, B. Goetz, P. Arya, et al. 2013. Protein tyrosine kinase regulation by ubiquitination: critical roles of Cbl-family ubiquitin ligases. *Biochim. Biophys. Acta.* 1833:122–139. https://doi.org/10.1016/j.bbamcr.2012.10.010

Monis, W.J., V. Faundez, and G.J. Pazour. 2017. BLOC-1 is required for selective membrane protein trafficking from endosomes to primary cilia. *J. Cell Biol.* 216:2131–2150. https://doi.org/10.1083/jcb.201611138

Mori, S., L. Claesson-Welsh, Y. Okuyama, and Y. Saito. 1995. Ligand-induced polyubiquitination of receptor tyrosine kinases. *Biochem. Biophys. Res. Commun.* 213:32–39. https://doi.org/10.1006/bbrc.1995.2094

Nielsen, B.S., R.R. Malinda, F.M. Schmid, S.F. Pedersen, S.T. Christensen, and L.B. Pedersen. 2015. PDGFRβ and oncogenic mutant PDGFRα D842V promote disassembly of primary cilia through a PLCγ- and AURKA-dependent mechanism. *J. Cell Sci.* 128:3543–3549. https://doi.org/10.1242/jcs.173559

Noda, K., M. Kitami, K. Kitami, M. Kaku, and Y. Komatsu. 2016. Canonical and noncanonical intraflagellar transport regulates craniofacial skeletal development. *Proc. Natl. Acad. Sci. USA.* 113:E2589–E2597. https://doi.org/10.1073/pnas.1519458113

Ocbina, P.J., J.T. Eggenschwiler, I. Moskowitz, and K.V. Anderson. 2011. Complex interactions between genes controlling trafficking in primary cilia. *Nat. Genet.* 43:547–553. https://doi.org/10.1038/ng.832

Olson, L.E., and P. Soriano. 2009. Increased PDGFRalpha activation disrupts connective tissue development and drives systemic fibrosis. *Dev. Cell.* 16:303–313. https://doi.org/10.1016/j.devcel.2008.12.003

Peschard, P., G. Kozlov, T. Lin, I.A. Mirza, A.M. Berghuis, S. Lipkowitz, M. Park, and K. Gehring. 2007. Structural basis for ubiquitin-mediated dimerization and activation of the ubiquitin protein ligase Cbl-b. *Mol. Cell.* 27:474–485. https://doi.org/10.1016/j.molcel.2007.06.023

Qin, J., Y. Lin, R.X. Norman, H.W. Ko, and J.T. Eggenschwiler. 2011. Intraflagellar transport protein 122 antagonizes Sonic Hedgehog signaling and controls ciliary localization of pathway components. *Proc. Natl. Acad. Sci. USA.* 108:1456–1461. https://doi.org/10.1073/pnas.1011410108

Rorsman, C., M. Tsioumpekou, C.H. Heldin, and J. Lennartsson. 2016. The Ubiquitin Ligases c-Cbl and Cbl-b Negatively Regulate Platelet-derived Growth Factor (PDGF) BB-induced Chemotaxis by Affecting PDGF Receptor β (PDGFRβ) Internalization and Signaling. *J. Biol. Chem.* 291:11608–11618. https://doi.org/10.1074/jbc.M115.705814

Ryan, P.E., G.C. Davies, M.M. Nau, and S. Lipkowitz. 2006. Regulating the regulator: negative regulation of Cbl ubiquitin ligases. *Trends Biochem. Sci.* 31:79–88. https://doi.org/10.1016/j.tibs.2005.12.004

Schneider, L., C.A. Clement, S.C. Teilmann, G.J. Pazour, E.K. Hoffmann, P. Satir, and S.T. Christensen. 2005. PDGFRαα signaling is regulated through the primary cilium in fibroblasts. *Curr. Biol.* 15:1861–1866. https://doi.org/10.1016/j.cub.2005.09.012

Schneider, L., C.M. Stock, P. Dieterich, B.H. Jensen, L.B. Pedersen, P. Satir, A. Schwab, S.T. Christensen, and S.F. Pedersen. 2009. The Na+/H+ exchanger NHE1 is required for directional migration stimulated via PDGFR-α in the primary cilium. *J. Cell Biol.* 185:163–176. https://doi.org/10.1083/jcb.200806019

Schneider, L., M. Cammer, J. Lehman, S.K. Nielsen, C.F. Guerra, I.R. Veland, C. Stock, E.K. Hoffmann, B.K. Yoder, A. Schwab, et al. 2010. Directional cell migration and chemotaxis in wound healing response to PDGF-AA are coordinated by the primary cilium in fibroblasts. *Cell. Physiol. Biochem.* 25:279–292. https://doi.org/10.1159/000276562

Schrøder, J.M., J. Larsen, Y. Komarova, A. Akhmanova, R.I. Thorsteinsson, I. Grigoriev, R. Manguso, S.T. Christensen, S.F. Pedersen, S. Geimer, and L.B. Pedersen. 2011. EB1 and EB3 promote cilia biogenesis by several centrosome-related mechanisms. *J. Cell Sci.* 124:2539–2551. https://doi.org/10.1242/jcs.085852

Seeger-Nukpezah, T., J.L. Little, V. Serzhanova, and E.A. Golemis. 2013. Cilia and cilia-associated proteins in cancer. *Drug Discov. Today Dis. Mech.* 10:e135–e142. https://doi.org/10.1016/j.ddmec.2013.03.004

Selbach, M., and M. Mann. 2006. Protein interaction screening by quantitative immunoprecipitation combined with knockdown (QUICK). *Nat. Methods.* 3:981–983. https://doi.org/10.1038/nmeth972

Taschner, M., and E. Lorentzen. 2016. The Intraflagellar Transport Machinery. *Cold Spring Harb. Perspect. Biol.* 8:a028092. https://doi.org/10.1101/cshperspect.a028092

Taschner, M., K. Weber, A. Mourão, M. Vetter, M. Awasthi, M. Stiegler, S. Bhogaraju, and E. Lorentzen. 2016. Intraflagellar transport proteins 172, 80, 57, 54, 38, and 20 form a stable tubulin-binding IFT-B2 complex. *EMBO J.* 35:773–790. https://doi.org/10.15252/embj.201593164

Umberger, N.L., and T. Caspary. 2015. Ciliary transport regulates PDGF-AA/αα signaling via elevated mammalian target of rapamycin signaling and diminished PP2A activity. *Mol. Biol. Cell.* 26:350–358. https://doi.org/10.1091/mbc.E14-05-0952

Velghe, A.I., S. Van Cauwenberghe, A.A. Polyansky, D. Chand, C.P. Montano-Almendras, S. Charni, B. Hallberg, A. Essaghir, and J.B. Demoulin. 2014. PDGFRA alterations in cancer: characterization of a gain-of-function V536E transmembrane mutant as well as loss-of-function and passenger mutations. *Oncogene.* 33:2568–2576. https://doi.org/10.1038/onc.2013.218

Vivar, O.I., G. Masi, J.M. Carpier, J.G. Magalhaes, D. Galgano, G.J. Pazour, S. Amigorena, C. Hivroz, and C.T. Baldari. 2016. IFT20 controls LAT recruitment to the immune synapse and T-cell activation in vivo. *Proc. Natl. Acad. Sci. USA.* 113:386–391. https://doi.org/10.1073/pnas.1513601113

Waterman, H., G. Levkowitz, I. Alroy, and Y. Yarden. 1999. The RING finger of c-Cbl mediates desensitization of the epidermal growth factor receptor. *J. Biol. Chem.* 274:22151–22154. https://doi.org/10.1074/jbc.274.32.22151